American Mineralogist, Volume 66, pages 1189–1201, 1981

A solution model for coexisting iron–titanium oxides

KHALIL J. SPENCER AND DONALD H. LINDSLEY

Department of Earth and Space Sciences
State University of New York
Stony Brook, New York 11794

Abstract

A solution model has been developed for coexisting magnetite–ulvöspinel and hematite–ilmenite solid solutions and applied to the Buddington–Lindsley (1964) geothermometer and oxygen barometer. The model is based on results from the hydrothermal experiments of Lindsley (550–1000°C), gas-mixing experiments of Katsura *et al.* (1976) and Webster and Bright (1961) (1000–1200°C), and new hydrothermal experiments performed by Spencer and Lindsley (1978) using the Co–CoO buffer. The model assumes (1) ilmenite$_{ss}$ behaves as a binary asymmetric Margules solution; (2) titanomagnetite behaves as a binary asymmetric Margules solution below 800°C and as an ideal binary solution above 800°C; (3) configurational entropy terms can be approximated by a molecular mixing model for magnetites, and by Rumble's (1977) model B (disorder of Fe^{3+}) for ($R\bar{3}$) ilmenites; (4) only ordered ($R\bar{3}$) ilmenite solutions are present.

The free energy of the exchange reaction $Fe_3O_4 + FeTiO_3 = Fe_2O_3 + Fe_2TiO_4$ and the excess parameters for each solution were solved by least-squares fit of the experimental data. The model has successfully reproduced experimental data in the temperature-f_{O_2} range 600–1300°C, bounded (approximately) by the nickel–nickel oxide and wüstite–magnetite buffer curves. The model predicts a consolute point for Mt–Usp of ~550°C at ~Usp 32 Mt 68. No attempt was made to estimate mathematically the Hem–Ilm two-phase field. Uncertainties in T and f_{O_2} are approximately 40–80°C and 0.5–1.0 log units f_{O_2} (2σ) assuming ±1% uncertainties in Usp$_{ss}$ and Ilm$_{ss}$ compositions.

Introduction

Since the introduction of the Mt$_{ss}$–Ilm$_{ss}$ (for list of abbreviations see Table 1) geothermometer–oxybarometer, most workers have utilized the graph of Lindsley (1963; Buddington and Lindsley, 1964, Fig. 5) to determine the temperature and oxygen fugacity of magnetite–ilmenite pairs. This graph has a number of drawbacks: (1) It involved interpolation between data obtained at a limited number of oxygen buffers, and this interpolation was largely intuitive; (2) for many Mt$_{ss}$–Ilm$_{ss}$ pairs—especially those from volcanic rocks—it is necessary to extrapolate the curves to higher temperatures or to higher oxygen fugacities, or both; and (3) the treatment of "minor constituents" such as Mn, Mg, Al, Cr, and V is necessarily arbitrary. Ideally one would like to know the effects of such constituents on the activities of Fe_2O_3 and $FeTiO_3$ in Ilm$_{ss}$ and of Fe_3O_4 and Fe_2TiO_4 in Mt$_{ss}$. An adequate solution model would eliminate these limitations—although additional experimental data would still be needed to assess quantitatively the effects of the minor constituents. We present here a solution model for coexisting Mt$_{ss}$ and Ilm$_{ss}$, based on a least-squares fit of thermodynamic parameters to experimental data obtained at 550 to 1200°C. We also include results from a new series of experiments on pure Fe–Ti oxides done using the Co–CoO oxygen buffer, which has improved our understanding of the phase relations between Mt$_{ss}$ and Ilm$_{ss}$ by permitting us to experiment in a region of T–f_{O_2} space previously inaccessible to well-calibrated oxygen buffer assemblages.

In the discussion that follows it is assumed that the Mt$_{ss}$ and Ilm$_{ss}$ are pure binary Fe–Ti oxides; no minor constituents are considered.

0003–004X/81/1112–1189$02.00

Table 1. Definition of symbols and abbreviations

$T^{\circ}C$, T(K) - Temperature in degrees Celsius or in Kelvin.

Mt - magnetite, Fe_3O_4. Usp - ulvospinel, Fe_2TiO_4.

Hem - hematite, Fe_2O_3. Ilm - ilmenite, $FeTiO_3$.

Mt_{ss} - solid solutions on or near the Mt-Usp join.

Ilm_{ss} - solid solutions on the Hem-Ilm join.

X_{Usp} - mole fraction of Usp in Mt_{ss} (= Usp/(Mt + Usp) for stoichiometric spinels; = 3 Ti/(Ti + Fe) for non-stoichiometric and/or oxidized spinels).

X_{Ilm} - mole fraction of Ilm in Ilm_{ss}; = Ilm/(Hem + Ilm).

γ_i - activity coefficient for component i.

$\underline{R}\bar{3}$ - space group of ordered Ilm_{ss}.

ΔG°_{exch} - molar Gibbs Free Energy of the exchange reaction (1).

ΔH°_{exch}, ΔS°_{exch} - molar enthalpy, entropy of the exchange reaction.

K_D - distribution coefficient, $(X_{Usp} \cdot X_{Hem})/(X_{Mt} \cdot X_{Ilm})$.

ΔG°_{ox} - molar Gibbs Free Energy of the oxidation reaction (3).

ΔG°_{Ilm} - molar Gibbs Free Energy of formation for ordered ($\underline{R}\bar{3}$) Ilm_{ss} from the oxides.

W^{Ilm}_G, W^{Hem}_G - asymmetric Margules parameters for excess Gibbs Free Energy of ordered ($\underline{R}\bar{3}$) Ilm_{ss}.

W^{Usp}_G, W^{Mt}_G - asymmetric Margules parameters for excess Gibbs Free Energy of Mt_{ss}.

Mt_{ss} (Ilm_{ss}) - Mt_{ss} in equilibrium with Ilm_{ss}.

fO_2 - oxygen fugacity. FMQ - fayalite-magnetite-quartz buffer.

MH - magnetite-hematite buffer. NNO - nickel-nickel oxide buffer.

WM - wustite-magnetite buffer. Co-CoO - cobalt-cobalt oxide buffer.

S_C - molar configurational entropy.

Previous work

Models

Rumble (1970) fitted a solution model to Carmichael's (1961) hematite–ilmenite miscibility gap, and using these data, refined excess parameters for magnetite–ulvöspinel solid solutions. Unfortunately, Carmichael's miscibility gap has since been shown to be excessively large (see Lindsley, 1976a) and the model must therefore be in error. Nevertheless, Rumble's separation of Mt–Ilm equilibria into oxidation and exchange reactions remains an important aspect of modeling this system.

Powell and Powell (1977) fitted a solution model to the NNO and FMQ experiments of Lindsley (1962, 1963), assuming that the $spinel_{ss}$ is ideal and that the $ilmenite_{ss}$ behaves according to Raoult's Law (for Ilm component) and Henry's Law (for Hem component). While their model appears to fit the distribution coefficients for the NNO and FMQ experiments, it has several drawbacks: it cannot predict the Mt–Usp miscibility gap, and it does not predict the results of experiments made using the more reducing buffer assemblages Co–CoO and WM at low (~600–800°C) temperatures, probably because of the increasing non-ideality of the solutions; thus it is only valid for a limited range of T and f_{O_2} (Fig. 1).

Phase equilibria

Hydrothermal exchange-equilibrium experiments in the range 550–1000°C have been done for the NNO, FMQ, and WM buffers by Lindsley (1962, 1963) and more recently using the Co–CoO buffer (Myers and Gunter, 1979; Chou, 1978) by Spencer and Lindsley (1978; Appendix 1). The results from these reversed experiments constitute the majority of the data used for our least-squares refinement.

Webster and Bright (1961, 1200°C), Taylor (1964, 1300°C) and Katsura *et al.* (1976, 1000–1200°C) have all performed 1-atmosphere experiments on Fe–Ti oxides using gas-mixing apparatus. Their results allow tie lines to be determined at temperatures higher than those permitted by standard hydrothermal techniques. Since the Mt_{ss}–Ilm_{ss} equilibria are not significantly affected by pressure in the 1–10 kbar range (Lindsley, 1963; Rumble, 1970), these 1-atmosphere experiments should be compatible with the hydrothermal experiments (670–2000 bars).

There are, however, some complicating factors that must be considered when using data from these high-temperature, low-pressure experiments. (1) The phase diagrams from Katsura *et al.* (1976), Webster and Bright (1961), and Taylor (1964) clearly show that the Mt_{ss} in equilibrium with Ilm_{ss} above 1000°C deviates significantly from the Mt–Usp binary toward the Ilm–Hem join. As the present model only considers binary spinels, we treated all the gas-mixing data by projecting spinel compositions along Fe/Ti isopleths onto the spinel join. This assumption will be discussed more fully below. (2) If a smooth curve is drawn from the low-temperature brackets up through the 1200°C and 1300°C data, the 1100° and 1000°C experiments of Katsura *et al.* (1976) appear to be too reduced near FMQ and NNO (Fig. 2). We suggest that the gas mixtures of Katsura *et al.* (1976) may not have reached equilibrium (see Huebner, 1975) so that the f_{O_2} values reported for their experiments were inac-

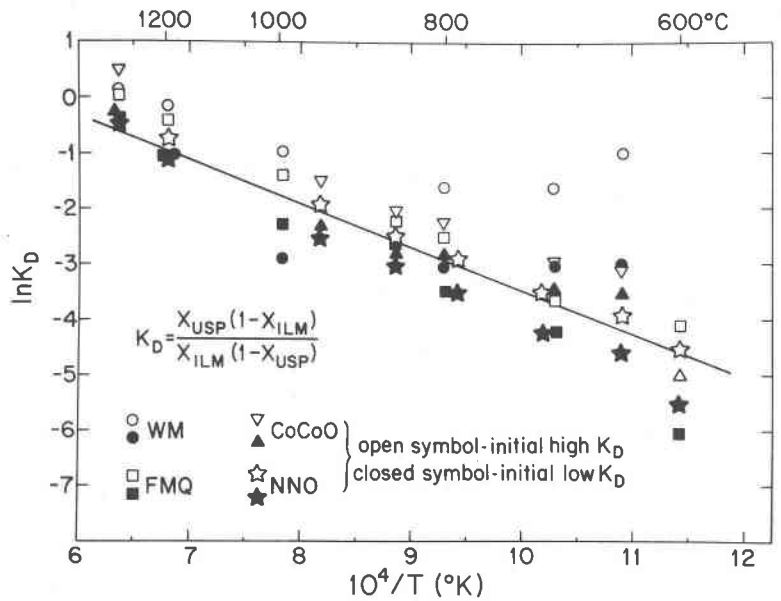

Fig. 1. Log K_D *vs.* $10^4/T$ plot of Fe–Ti oxide experiments, where K_D is defined as shown. Data from 600°C to 1000°C are reversed hydrothermal experiments of Lindsley (1962, 1963) and Spencer and Lindsley (1978); the wüstite–magnetite "reversals" are constrained by the hydrothermal experiments and by the iron-saturated compositions for Fe–Ti oxides shown by Simons and Woermann (1978). Data above 1000°C are not reversals, but are the authors' estimates of the uncertainty (experimental and that due to our interpolations) of 1300°C Taylor (1964) and 1200°C Webster and Bright (1961) and Katsura *et al.* (1976) experimental data.

curate. Consequently, we have not used data from Katsura *et al.* (1976) for 1000° and 1100° in fitting our model.

The solution model

The compositions of coexisting Mt_{ss} and Ilm_{ss} are governed by a temperature-dependent exchange reaction and an oxidation reaction (Rumble, 1970). The exchange reaction can be written as:

$$Fe_3O_4(Mt) + FeTiO_3(Ilm) = Fe_2TiO_4(Mt) + Fe_2O_3(Ilm) \quad (1)$$

for which

$$-\frac{\Delta G^\circ_{exch}}{RT} = \ln\left[\frac{X^\alpha_{Usp}(1-X_{Ilm})^\alpha}{(1-X_{Usp})^\alpha X^\alpha_{Ilm}}\right] + \ln\left[\frac{\gamma^\alpha_{Usp}\cdot\gamma^\alpha_{Hem}}{\gamma^\alpha_{Mt}\cdot\gamma^\alpha_{Ilm}}\right] \quad (2)$$

and the oxidation reaction as:

$$4Fe_3O_4(Mt) + O_2 = 6Fe_2O_3(Ilm) \quad (3)$$

with

$$-\frac{\Delta G^\circ_{ox}}{RT} = \ln\left[\frac{X^{6\cdot\alpha}_{Hem}}{X^{4\cdot\alpha}_{Mt}}\right] + \ln\left[\frac{\gamma^{6\cdot\alpha}_{Hem}}{\gamma^{4\cdot\alpha}_{Mt}}\right] - \ln f_{O_2} \quad (4)$$

where

$$\Delta G^\circ_{exch} = \Delta G^\circ_f(Usp) + \Delta G^\circ_f(Hem) - \Delta G^\circ_f(Mt) - \Delta G^\circ_f(Ilm) \quad (5)$$

$$\Delta G^\circ_{ox} = 6\Delta G^\circ_f(Hem) - 4\Delta G^\circ_f(Mt) \quad (6)$$

The equations for the total free energy of the solid solutions are:

$$G_{TOT}(Usp_{ss}) = \mu^\circ_{Usp}X_{Usp} + \mu^\circ_{Mt}X_{Mt} + \alpha RT(X_{Usp}\ln X_{Usp} + X_{Mt}\ln X_{Mt}) + W^G_{Usp}X^2_{Mt}X_{Usp} + W^G_{Mt}X^2_{Usp}X_{Mt} \quad (7)$$

$$G_{TOT}(Ilm_{ss}) = \mu^\circ_{Ilm}X_{Ilm} + \mu^\circ_{Hem}X_{Hem} + \alpha RT(X_{Ilm}\ln X_{Ilm} + X_{Hem}\ln X_{Hem}) + W^G_{Ilm}X^2_{Hem}X_{Ilm} + W^G_{Hem}X^2_{Ilm}X_{He} \quad (8)$$

The α terms have been set equal to 2 for ilmenite and 1 for titanomagnetite in accordance with the

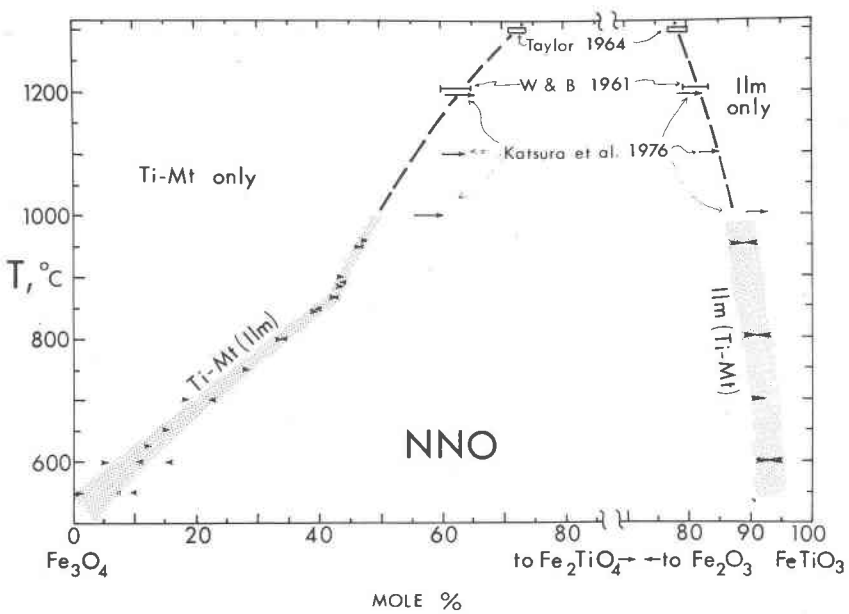

Fig. 2. Plot of experiments using the NNO buffer. 500–1000°C results are from Lindsley (1962, 1963). Compositions above 1000°C are our interpolations based on experiments of Taylor (1964) (1300°C), Webster and Bright (1961) (1200°C), Katsura, *et al.* (1976) (1000–1200°C). The Katsura *et al.* 1000° and 1100° data appear to be too reduced with respect to the other experiments. Diagram shows our suggested "kink" in Mt_{ss}(Ilm) between 800° and 900°C.

configurational entropy expressions (Rumble, 1977) that we have adopted. These values are discussed more fully in a later section.

In these equations, the mole fractions of Usp, Ilm, Mt, Hem are known from the experiments. The unknowns are ΔG°_{exch} (actually expressed as G°_f(Usp) for reasons explained below), and the four activity coefficients. One can therefore write two equations in five unknowns (equations 2 and 4) for each experimental Mt–Ilm pair and, having solved for these unknowns, use the thermodynamic data to write analytical expressions for the geothermometer and oxygen barometer. ΔG°_{ox} is the standard free energy of the MH buffer assemblage (Haas, cited by Huebner, 1971); the ΔG°_f for Ilm and Mt (from the oxides) are taken from Robie *et al.*, 1978; G°_f(Hem) ≡ 0. We assume that the activity coefficients are functions of temperature and composition, and have chosen to re-cast these as linear functions of temperature in the form of binary asymmetric Margules parameters, *i.e.*,

$$\alpha RT \ln \gamma_i = X_j^2(W_{Gi} + 2X_i(W_{Gj} - W_{Gi})) \quad (9)$$

where i, j are the two end members of a solid solution (Thompson, 1967) and where

$$W_{G(i)} = W_{H(i)} - TW_{S(i)}. \quad (10)$$

Since data on the free energy of formation of the end-members may be of uneven quality and the degree of normal-inverse character of the spinel end-members uncertain, we similarly solved for ΔG°_{exch} in terms of the free energy of formation of Usp as

$$\Delta G^\circ_f(\text{Usp}) = \Delta H^\circ_f(\text{Usp}) - T\Delta S^\circ_f(\text{Usp}). \quad (11)$$

Magnetite-ulvöspinel solid solutions

Buddington and Lindsley (1964, p. 314–322) summarized the reasons for believing that deviation of spinel compositions from the Mt–Usp join toward the Hem–Ilm join is negligible below 1000°C. But experiments at 1300°C (Taylor, 1964) and at 1200°C (Webster and Bright, 1961; Katsura *et al.*, 1976) show that, at least for low pressures, pure Mt_{ss} (Ilm_{ss}) clearly deviates nonstoichiometrically from the Mt–Usp join towards the Hem–Ilm join above 1000°C. There are, however, difficulties in formally treating Mt_{ss} as a ternary solution: (1) It is by no means clear what third component should be used in order to yield appropriate activity coefficients for Fe_3O_4 and Fe_2TiO_4, and (2) for natural magnetites that have undergone subsolidus oxidation, or for those that are analyzed by electron microprobe—and the great majority fall into one or both of these

categories—both the initial Fe_2O_3 content and therefore the extent of cation deficiency are unknown. Thus even with a scheme for treating synthetic Fe–Ti magnetites as ternary solutions, it would be difficult or impossible to treat most natural Fe–Ti spinels. For these reasons, we have chosen to project the compositions of natural and synthetic cation-deficient magnetites along Fe/Ti isopleths onto the Mt–Usp join, as for example composition M to M″ in Figure 3. This is the convention employed by Buddington and Lindsley (1964) and most other workers, but not by Anderson (1968) or by Katsura *et al.* (1976). The projected compositions are then treated as if they were truly binary Mt–Usp solid solutions. This treatment is justified at least in an empirical sense: the solution model correctly predicts the compositions of the 1200°C experiments of Katsura *et al.* (1976) and of Webster and Bright (1961) and closely approaches the compositions of the 1300°C experiments of Taylor (1964) when spinel compositions are projected in this way.

Ordering of Fe^{2+}–Fe^{3+}–Ti^{4+} cations on the tetrahedral and octahedral sites of the spinel structure has been suggested by various workers (O'Reilly and Banerjee, 1965; Banerjee and O'Reilly, 1966; Akimoto, 1954; Neel, 1955; Chevallier *et al.*, 1955; Bleil, 1971, 1976; Stephenson, 1969; Wechsler, 1981; see Lindsley, 1976b, for a review). Although work by Stephenson (1969) and Bleil (1971, 1976) suggested a temperature-dependent ordering scheme for Fe^{2+}/Fe^{3+} cations, their assumptions were not required by the data, and recent work by O'Donovan and O'Reilly (1979) and Wechsler (1981) failed to find evidence for a temperature-dependent cation distribution.

Several temperature-independent models of Fe^{2+}, Fe^{3+}, and Ti mixing have been suggested, all of which require the Ti to remain on the octahedral sites. O'Reilly and Banerjee (1965) suggest a model which is intermediate between the Akimoto distribution and the Neel–Chevallier distribution, and requires abrupt breaks in the cation distribution and configurational entropy at $X(\text{Usp}) = 0.2$ and 0.8, breaks that are not discernable in the phase equilibrium data or in the crystallographic studies of Wechsler (1981), who suggests that the s-shaped $a_{\text{cell edge}}$ *vs.* X_{Usp} curve may be due to factors such as Ti–Ti octahedral repulsion, especially at higher Ti contents. Rumble (1970) and Powell and Powell (1977) used a molecular model, the latter authors suggesting that strong short-range order in Ti-magnetites decreases the free energy contribution expected from mixing cations on the two distinct spinel sites. The molecular model yields an $\alpha = 1$ for the spinel phase in equations 2, 4, and 7.

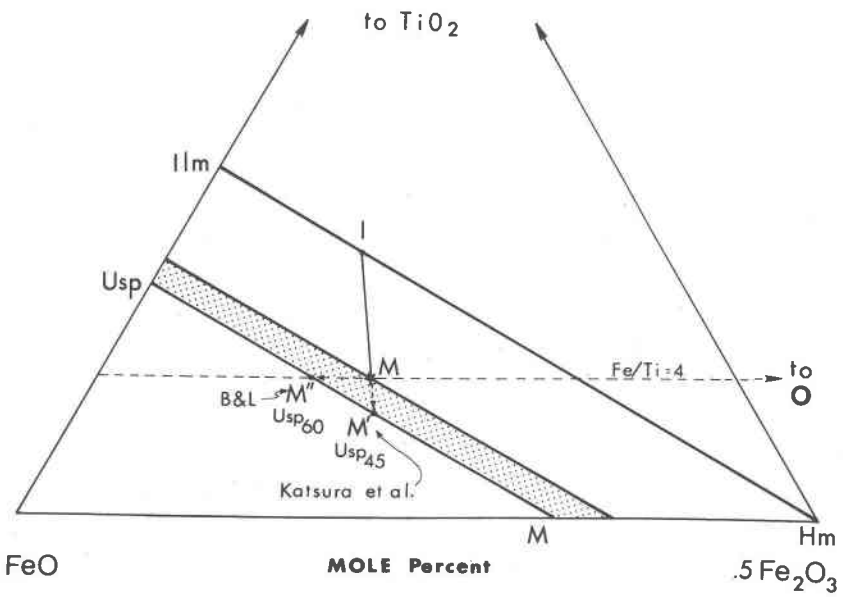

Fig. 3. Schematic high temperature phase diagram showing the width of the phase field of Usp–Mt solid solutions. "True" composition M would be projected along line of constant Fe:Ti to M'' by Buddington and Lindsley (1964), and this paper. Katsura *et al.* (1976) project to M′, although this could not be justified for microprobe results, which do not measure Fe_2O_3 content.

Wechsler (1981) has suggested an Akimoto distribution (with possible hints of short-range order) based on powder X-ray and neutron diffraction studies of synthetically grown wüstite-saturated Ti-magnetites. The Akimoto distribution corresponds to $\alpha = 2$; short-range order would decrease this value.

There is some evidence, however, for an abrupt change in the free energy curve of Mt_{ss} in the vicinity of 850°C. Inflections in *T–X* space shown by diagrams of Mt_{ss}(Ilm) for NNO, FMQ (Buddington and Lindsley, 1964, Fig. 2, p. 313 and Fig. 2, this paper), and plots of $\ln K_D$ *vs.* $1/T$ (Fig. 1) showing changes in slope near 850°C, suggest a change in the thermodynamic properties of the Mt solution.

In the absence of conclusive data on the distribution of cations in the spinel solution, we have chosen to retain the simpler $RTX\ln X$ formulation for magnetite solid solutions and estimate the change in excess free energy above and below 800°C using potentially different sets of excess parameters for magnetite solid solutions. We attempted to fit models assuming $\alpha = 1$ and $\alpha = 2$ (Akimoto distribution) for the spinel phase. The $\alpha = 1$ model provided a better overall fit to the data and gave a lower estimate (550°C) of the crest of the magnetite–ulvöspinel miscibility gap than did the $\alpha = 2$ model (620°C). The lower value is in better agreement with recent estimates of the magnetite_{ss} solvus given by Lindsley (1981) and Price (1981). In addition, the $\alpha = 1$ model was consistent with magnetite_{ss} behaving ideally above 800°C, whereas the $\alpha = 2$ version required a positive excess energy. We therefore accepted a "molecular" magnetite solid solution incorporating binary asymmetric excess parameters below and behaving ideally above 800°C. Contributions to the free energy of the magnetite solutions arising from the configurational entropies of the spinel end-members have been compensated by refining ΔG°_{exch} as an unknown.

Ilmenite solutions

Ilmenite solid solutions in equilibrium with magnetite appear always to be stoichiometric and binary. Pure hematite and hematite-rich solutions have the disordered $R\bar{3}c$ structure, but intermediate compositions have been shown to be ordered or disordered, depending on their thermal history. Pure ilmenite has the ordered $R\bar{3}$ structure with distinct A and B layers, and appears to retain this structure up to at least 1050°C (Wechsler, 1978), as do ilmenites close to $FeTiO_3$. Most natural ilmenites, and the experimental ilmenites used in our study, are sufficiently $FeTiO_3$-rich that they should have crystallized in the ordered $R\bar{3}$ form. For these reasons, this model only concerns itself with ordered $R\bar{3}$ ilmenites—the $R\bar{3}/R\bar{3}c$ order–disorder phenomenon is not considered. Although some of the 1200°C ilmenite compositions used in our data base may be considerably disordered, our model correctly predicts the 1200°C phase compositions leading us to believe that any disordering in these ilmenites has been effectively described by the excess parameters.

Even within the $R\bar{3}$ region, ordering of Fe^{2+}–Fe^{3+} on the A and remaining B sites is possible (see Rumble, 1977, for a review of Ilm–Hem configurational entropy). The existence of superexchange coupling and electrostatic repulsion could give rise to Ti^{4+} coupling to Fe^{2+}, and Fe^{3+} to Fe^{3+} across intervening oxygen layers, resulting in a "molecular" substitution (as suggested implicitly by Rumble, 1970; Powell and Powell, 1977) and a configurational entropy of

$$S_c = -R(X\ln X + (1-X)\ln(1-X)). \quad (12)$$

If Fe^{3+} and Ti^{4+} mix randomly on the B-sites and Fe^{2+}–Fe^{3+} mix randomly on the A sites (Rumble, 1977, model B), the configurational entropy is

$$S_c = -2R(X\ln X + (1-X)\ln(1-X)). \quad (13)$$

If Ti remains on the B-sites with Fe^{2+} and Fe^{3+} free to mix randomly on the A and remaining B sites (only Ti being restricted), we have

$$S_c = -R\left[\left(\frac{X}{2-X}\right)\ln\left(\frac{X}{2-X}\right) + \left(\frac{X-X^2}{2-X}\right)\ln\left(\frac{X-X^2}{2-X}\right) + \left(\frac{2-2X}{2-X}\right)\ln\left(\frac{2-2X}{2-X}\right) + \frac{2(1-X)^2}{(2-X)}\ln\left(\frac{2(1-X)^2}{2-X}\right) + X\ln X\right] \quad (14)$$

All of these cases were considered in formulating the model. Models incorporating equation 12 proved unable to fit the experimental data collected at low f_{O_2} values even considering the wide brackets for experiments at WM buffer. Models incorporating 13 and 14 were both successful in reproducing the data; the width of the Ilm–Hem hydrothermal

brackets prevented us from rejecting one or the other, since we could fit either case by varying the Ilm_{ss} mole fractions within the experimentally-determined brackets. Since the cation distribution for intermediate ilmenites is not well known, we have accepted equation 13 because of its more successful fit to the data compared to 12 and its simpler activity–composition relationships compared to 14.

Free energy of the exchange reaction

Data are available for the free energy of formation of Fe_3O_4, Fe_2TiO_4, Fe_2O_3, and $FeTiO_3$. One could combine these data algebraically so as to obtain ΔG°_{exch} for reaction 1. However, because the data were obtained by a variety of techniques and may be of different quality, we chose to refine ΔG°_{exch} as an unknown during the least-squares fitting. In practice the tabulated values for ΔG°_f of Fe_3O_4, Fe_2O_3, and $FeTiO_3$ (relative to the oxides) from Robie *et al.* (1978) were accepted and fitted to straight lines of the form $\Delta G^\circ = \Delta H^\circ - T\Delta S^\circ$. The actual terms refined therefore were

$$\Delta H^\circ_{Mt} + \Delta H^\circ_{Ilm} - \Delta H^\circ_{Hem} + \Delta H^\circ_{exch} \qquad (15)$$

and

$$\Delta S^\circ_{Mt} + \Delta S^\circ_{Ilm} - \Delta S^\circ_{Hem} + \Delta S^\circ_{exch} \qquad (16)$$

which should correspond to ΔH°_{Usp} and ΔS°_{Usp}. An advantage to this approach is that it compensates for any uncertainties in the evaluation of configurational entropy terms for the spinel end-members (see Walbaum, 1973, p. 48–50, for a discussion of this problem).

The reader should note, however, that the ΔH° and ΔS° for Usp in Table 2 are the intercept and slope of a line on a G°_f–T plot, and *not* values for 298K.

Oxygen buffers

In order to apply the hydrothermal experimental data to the oxidation equation 4, the oxygen fugacities of the MH, NNO, FMQ, Co–CoO, and WM buffers must be known. We have used the following buffer calibrations in fitting the solution model: Haas (as cited by Huebner, 1971) for MH, Huebner and Sato (1970) for NNO, Chou and Williams (1977) for FMQ, and Chou (1978) for Co–CoO. Two calibrations of WM—Darken and Gurry (1946, 1050–1300°C) and Rizzo *et al.* (1969, 700–925°C; 900–1200°C)—were tested, and the Rizzo values provided a better fit at low temperatures (<800°C). Since ordering changes in wüstite may occur at low temperatures (Vallet, 1975, Fender and Riley, 1969, Koch and Cohen, 1969), extrapolation of Darken and Gurry's high-temperature measurements to such low temperature seems inappropriate, and we have used Rizzo's calibration.

Modeling

Based on the above assumptions, a 10-parameter solution model was refined; the variables and their refined values are listed in Table 2; and the correlation coefficients in Table 3. Each experimentally determined tie line was expressed as an exchange reaction and oxidation reaction (equations 2 and 4), with equations 9 and 10 substituted appropriately, rewritten as a set of linear equations in the 10 unknowns (with the W-terms for Usp_{ss} being set $\equiv 0$ above 800°C) and solved by computer least-squares fit. The fitting program was adopted from Duffy (1977) which finds the least squares minimum by singular-value decomposition using subroutine SOLSVD (Computing Center, University of British Columbia).

The initial data used as input to the model were the midpoints from the Lindsley (1962, 1963) and Spencer and Lindsley (1978) composition brackets for hydrothermal experiments, and projections of the Webster and Bright (1961) and Katsura *et al.* (1976) tie lines. These initial attempts resulted in large model residuals ($A\bar{x} - \bar{b}$) for many data pairs. To reduce these residuals, the compositional data (X_{Usp} and X_{Ilm}) were adjusted *within* the experimental brackets until the residuals were reduced to a manageable level. Adjusting the mole fractions within experimental brackets is permissible since properly determined brackets only require that the equilibrium values for compositions lie somewhere inside the brackets. This procedure is equivalent to a non-linear least-squares solution for the best

Table 2. Solution model parameters (in Joules)

W^{Usp}_G ($T \geq 800$°C) $\equiv 0$	W^{Mt}_G ($T \geq 800$°C) $\equiv 0$
W^{Usp}_H ($T < 800$°C) = 64835 (3665)	W^{Usp}_S ($T < 800$°C) = 60.296 (3.618)
W^{Mt}_H ($T < 800$°C) = 20798 (2079)	W^{Mt}_S ($T < 800$°C) = 19.652 (2.070)
W^{Ilm}_H = 102374 (3314)	W^{Ilm}_S = 71.095 (2.585)
W^{Hem}_H = 36818 (519)	W^{Hem}_S = 7.7714 (0.4368)
ΔH°_{Usp} = -3073.1 (1205)*	ΔS°_{Usp} = 10.724 (1.038)*

* Refined using Robie et al. (1978) values for ΔG°_f(Ilm), ΔG°_f(Mt) (oxides reference state).

Table 3. Correlation matrix

	W_H(Usp)	W_S(Usp)	W_H(Mt)	W_S(Mt)	W_H(Ilm)	W_S(Ilm)	W_H(Hem)	W_S(Hem)	ΔH^o_f(Usp)	ΔS^o_f(Usp)
W_H(Usp)	1.000									
W_S(Usp)	0.994	1.000								
W_H(Mt)	-0.397	-0.396	1.000							
W_S(Mt)	-0.406	-0.410	0.991	1.000						
W_H(Ilm)	-0.168	-0.188	-0.287	-0.205	1.000					
W_S(Ilm)	-0.162	-0.181	-0.297	-0.218	0.994	1.000				
W_H(Hem)	0.171	0.171	0.375	0.301	-0.836	-0.850	1.000			
W_S(Hem)	0.165	0.169	0.372	0.308	-0.784	-0.812	0.986	1.000		
ΔH^o_f(Usp)	-0.407	-0.377	0.152	0.153	0.030	0.022	-0.137	-0.124	1.000	
ΔS^o_f(Usp)	-0.377	-0.348	0.139	0.139	0.021	0.013	-0.127	-0.115	0.990	1.000

values of both the thermodynamic parameters and the compositions of the coexisting pairs.

Since the SVD routine is capable of refining parameters for a nearly singular matrix, we assured ourselves that trivial parameters were not produced by re-refining the final data with a program that computed the inverse directly. This produced a well-behaved inverse with parameters very similar to those reported here.

5). Readers will note only negligible differences between the old and new curves in the vicinity of the NNO and FMQ buffers from 600–1000°C; but the new curves should definitely be superior in other regions. The stippled boundaries are our suggestions of the valid range of the model.

The temperature at which a magnetite–ilmenite pair equilibrated can be calculated from the following equation:

$$T(^\circ\mathrm{K}) = \frac{(-\mathrm{Al}\cdot W_H^{\mathrm{Usp}} - \mathrm{A2}\cdot W_H^{\mathrm{Mt}} + \mathrm{A3}\cdot W_H^{\mathrm{Ilm}} + \mathrm{A4}\cdot W_H^{\mathrm{Hem}} + \Delta H^\circ_{\mathrm{exch}})}{(-\mathrm{Al}\cdot W_S^{\mathrm{Usp}} - \mathrm{A2}\cdot W_S^{\mathrm{Mt}} + \mathrm{A3}\cdot W_S^{\mathrm{Ilm}} + \mathrm{A4}\cdot W_S^{\mathrm{Hem}} + \Delta S^\circ_{\mathrm{exch}} - R\cdot \ln K^{\mathrm{exch}})} \quad (17)$$

Revised f_{O_2} relations for coexisting Mt_{ss} + Ilm_{ss}

The solution model has been used to revise the Mt_{ss}–Ilm_{ss} geothermometer–oxybarometer. Figure 4 shows our revised T–f_{O_2} curves calculated from the model. The revised curves were derived by plotting a large number of X_{Usp} and X_{Ilm} values *vs.* T and $\ln f_{O_2}$; these compositions were determined using the solution model parameters, and hence all interpolations and extrapolations are in accord with the model[1]. Figure 4 completely supersedes the earlier graph (Buddington and Lindsley, 1964, Fig.

where $\Delta H^\circ_{\mathrm{exch}} = 27799$ Joules/mole

$\Delta S^\circ_{\mathrm{exch}} = 4.1920$ Joules/mole-degree

$\mathrm{Al} = -3X^2_{\mathrm{Usp}} + 4X_{\mathrm{Usp}} - 1$

$\mathrm{A2} = 3X^2_{\mathrm{Usp}} - 2X_{\mathrm{Usp}}$

$\mathrm{A3} = -3X^2_{\mathrm{Ilm}} + 4X_{\mathrm{Ilm}} - 1$

$\mathrm{A4} = 3X^2_{\mathrm{Ilm}} - 2X_{\mathrm{Ilm}}$

$K^{\mathrm{exch}} = (X_{\mathrm{Usp}}\cdot X^2_{\mathrm{Hem}})/(X_{\mathrm{Mt}}\cdot X^2_{\mathrm{Ilm}})$ (18)

We suggest using the low-T parameters to calculate an initial temperature, and if temperature is above 800°C setting the Mt_{ss} W_G's ≡ 0 and recalulating T.

The oxygen fugacity can similarly be calculated using the relationship:

$$\log_{10} f_{O_2} = \mathrm{MH} + (12\ln(1 - X_{\mathrm{ilm}}) - 41\ln(1 - X_{\mathrm{Usp}}) + (1/RT)(8X^2_{\mathrm{Usp}}(X_{\mathrm{Usp}} - 1)\cdot W_G^{\mathrm{Usp}}$$

[1]For a given temperature, values for (X_{Mt} or X_{Ilm}) were assumed as knowns and those of (X_{Ilm} or X_{Mt}) were determined using the exchange-equilibrium condition. Since coexisting compositional terms were solved in terms of activity coefficients that are themselves functions of composition, an iterative computing procedure was used that converged on the compositions. Values for f_{O_2} were then calculated on the basis of these values of T, X_{Hem}, and X_{Mt} using the oxidation reaction condition.

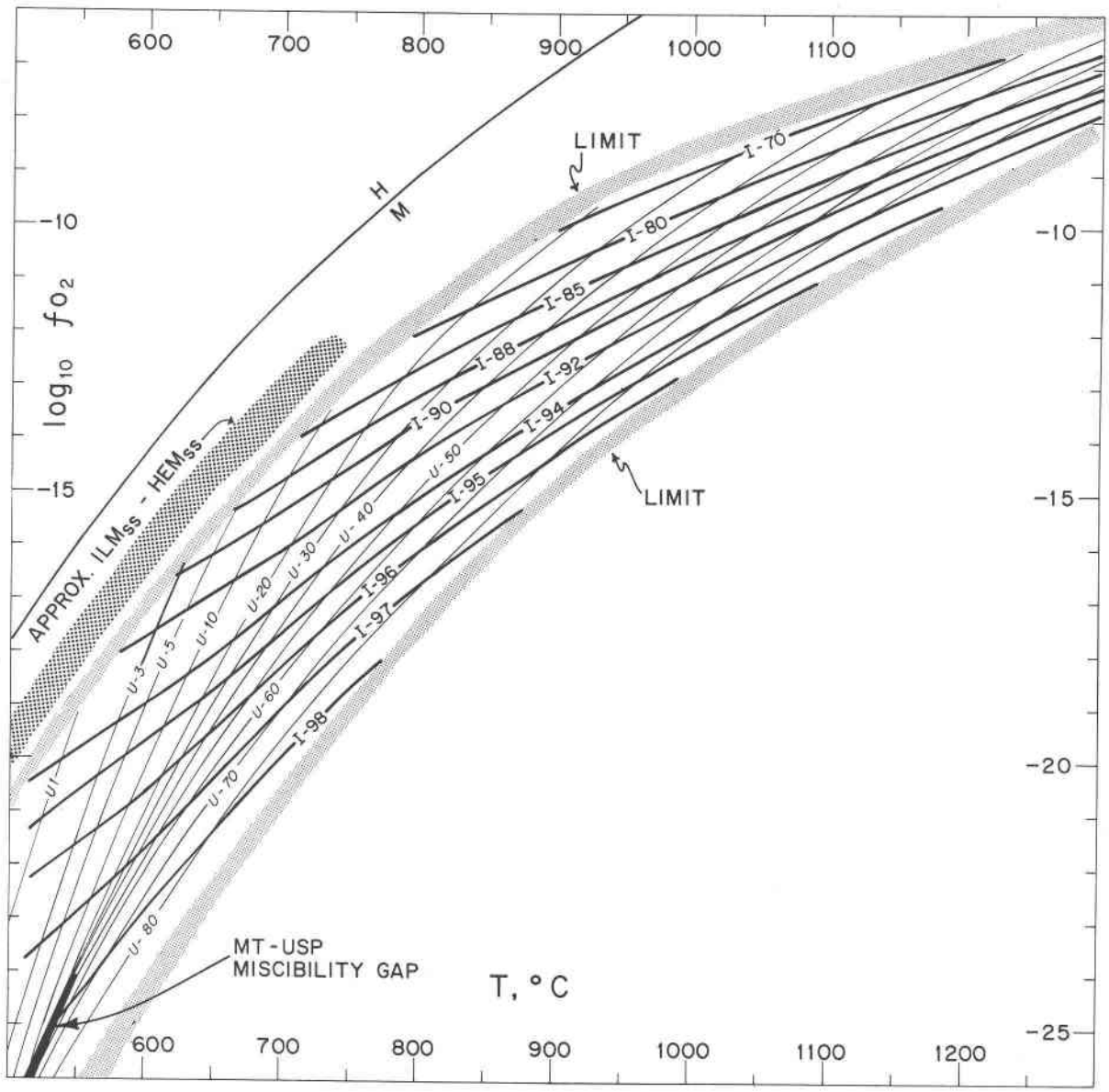

Fig. 4. T–f_{O_2} grid for coexisting Mt_{ss}–Ilm_{ss} pairs, based on the solution model. The stippled fields are our estimates of the limits of the model. The Mt–Usp miscibility gap is that calculated by the model for the three-phase assemblage Mt_{ss} + Usp_{ss} + Ilm_{ss}. The Ilm–Hem miscibility gap (labeled "Approx. $ILM_{ss}HEM_{ss}$") is our best guess from experimental data—it is *not* calculated.

$$+ 4X_{Usp}^2(1 - 2X_{Usp})\cdot W_G^{Mt} + 12X_{Ilm}^2(1 - X_{Ilm}) \cdot W_G^{Ilm} - 6X_{Ilm}^2(1 - 2X_{Ilm})\cdot W_G^{Hem}))/2.303 \quad (19)$$

T is calculated from the geothermometer equation and used to evaluate the W_G's; MH is the Haas value for the log of the oxygen fugacity of magnetite-hematite at the specific temperature of interest ($\log_{10}MH = 13.966 - 24634/T$). A small BASIC program that calculates T, f_{O_2}, and their uncertainties from X_{Usp}, X_{Ilm}, σX_{Usp} and σX_{Ilm} has been written and is available from the authors.

Uncertainties in T and f_{O_2} are calculated from the estimated standard errors for the solution parameters, the correlation matrix of solution parameters, and estimates of the uncertainty of compositional data. Since σ_T and σ_{fO_2} are functions of both composition and model parameters, a range of values for each is possible (formulations for calculating σ_T and σ_{fO_2} are included in program TFO_2).

Assuming that 2σ compositional uncertainties are ± 1 mole percent for Ilm_{ss} and Mt_{ss}, we find that the ranges of error on T and f_{O_2} are approximately 40–80°C and 0.5–1.0 log units (2σ errors). Of this error, uncertainties due to the parameters are ~10–35°C; 0.10–0.20 log units f_{O_2}, with the remainder due to uncertainties in the compositions entered by the user.

The form of the two-phase regions (Mt–Usp and Hem–Ilm) shown in Figure 4 deserves comment. The Mt–Usp gap is that calculated from the solution model for the three-phase assemblage Mt_{ss} + Usp_{ss} + Ilm_{ss}. The compositions and critical temperature agree moderately well with approximate determinations of the gap (Vincent *et al.*, 1957; Basta, 1960; Price, 1981; Lindsley, 1981), but the reader should bear in mind that the gap in Figure 4 is calculated only and not confirmed experimentally. Furthermore, even if the Mt–Usp gap in Figure 4 were rigorously correct for Mt_{ss} + Usp_{ss} in equilibrium with Ilm_{ss}, it is quite possible that the two spinels *without* Ilm_{ss} could coexist at slightly different values of T and f_{O_2}.

It is perhaps objectionable to use the term "miscibility gap" as applied to coexisting $Hem_{ss}(R\bar{3}c)$ and $Ilm_{ss}(R\bar{3})$, since the different space groups suggest that there are two different solutions. The Hem_{ss}–Ilm_{ss} two-phase field must almost certainly lie within the finely stippled area, based on a variety of constraints, but its actual position has been neither measured nor calculated.

Activity coefficients for Mt_{ss} and for Ilm_{ss}

It is possible to substitute appropriate Margules parameters from Table 1 into equations 9 and 10 and to calculate activity coefficients for Fe_3O_4 and Fe_2TiO_4 in Mt_{ss} and for Fe_2O_3 and $FeTiO_3$ in Ilm_{ss} ($R\bar{3}$ solutions only). While these terms may be very useful, they probably are not rigorously correct. As mentioned, the excess (Margules) terms in our model probably contain effects that should strictly have been included in configurational entropy and enthalpy terms for each solution, except that we do not know the cation distributions in detail. Since both solutions are being solved simultaneously, the refined excess terms of each may be affected by inaccurate assumptions about the other. The activity coefficients are internally consistent and applicable within the system FeO–Fe_2O_3–TiO_2, but they may not be valid in more extended systems or if used independently of one another.

Summary and conclusions

A solution model has been developed by least-squares fitting of 10 parameters—5 temperature-independent and 5 temperature-dependent terms—to experimental data obtained at 550–1000°C and at 1200°C. The model is based on a number of assumptions:

(1) Both Mt_{ss} and Ilm_{ss} ($R\bar{3}$) behave as asymmetric binary solutions.

(2) Non-stoichiometry of Mt_{ss} (Ilm_{ss}) above 1000°C can be accounted for by projecting the true cation-deficient composition along a line of constant Fe–Ti ratio onto the binary Mt–Usp join.

(3) Contributions to the Gibbs free energy of Mt_{ss} and Ilm_{ss} from configurational entropy and ordering can be approximated by simple $\alpha R(X\ln X)$ terms. This assumption probably is not correct in detail, but is mandated given our present lack of detailed knowledge regarding cation distributions in Mt_{ss} and in Ilm_{ss} as functions of temperature.

(4) A model for $R\bar{3}$ ilmenites that assumes disorder of (Fe^{2+} + Fe^{3+}) on the A-sites and (Fe^{3+} + Ti) on the B-sites ($\alpha = 2$) gives a better fit to the phase equilibria data than one assuming a "molecular" solution ($\alpha = 1$), and is simpler than one (of equivalent goodness-of-fit) assuming complete Fe^{2+}–Fe^{3+} disorder.

(5) Changes in solution behavior near 800–850°C for NNO, FMQ, and Co–CoO buffers are caused by abrupt changes in Gibbs free energy of Mt_{ss}, hence different expressions for G_{TOT} (Mt_{ss}) are used above and below that temperature. Above 800°C, an ideal model satisfies the data, while below 800°C, temperature-dependent (W_H–TW_S) terms are needed.

Acknowledgments

We thank John Grover, Roger Powell, Douglas Rumble III, Richard Reeder, Barry Wechsler, Dave Anderson, and Paula Davidson for reviews and discussions of this manuscript. We thank Robin Spencer for typing too many versions of this paper. This work was supported by NSF, Earth Science Section, Grant No. EAR 7622129.

Lindsley also is deeply grateful to Hugh Greenwood, Tom Brown, and the Department of Geological Sciences, University of British Columbia, where the work was started during a sabbatical leave.

References

Akimoto, S. (1954) Thermo-magnetic study of ferromagnetic minerals contained in igneous rocks. Journal of Geomagnetics and Geoelectricity, 6, 1–14.

Albee, A. L. and Ray, L. (1970) Correction factors for electron probe microanalysis of silicates, oxides, carbonates, phosphates, and sulfates. Analytical Chemistry, 42, 1408–1414.

Anderson, A. T. (1968) Oxidation of the LaBlanche Lake titaniferous magnetite deposit, Quebec. Journal of Geology, 76, 528–547.

Banerjee, S. K. and O'Reilly, W. (1966) Coercivity of Fe^{++} in octahedral sites of Fe–Ti spinels. IEEE, Transactions Magnetics Magazine, 2, 463–467.

Basta, E. Z. (1960) Natural and synthetic titanomagnetites (the system Fe_3O_4–Fe_2TiO_4–$FeTiO_3$) Neues Jahrbuch für Mineralogie Abhandlungen, 94, 1017–1048.

Bence, A. E. and Albee, A. L. (1968) Empirical correction factors for the electron microanalysis of silicates and oxides. Journal of Geology, 76, 382–403.

Bleil, U. (1971) Cation distribution intitanomagnetites, Zeitschrift für Geophysik, 37, 305–319.

Bleil, U. (1976) An experimental study of the titanomagnetite solid solution series, Pure and Applied Geophysics, 114, 165–175.

Buddington, A. F. and Lindsley, D. H. (1964) Iron–titanium oxide minerals and synthetic equivalents. Journal of Petrology, 5, 310–357.

Carmichael, C. M. (1961) The magnetic properties of ilmenite–hematite crystals. Proceedings of the Royal Society, A263, 508–530.

Chevallier, R., Bolfa, T., and Mathieu, S. (1955) Titanomagnetites et ilmenites ferromagnetiques. (1) Etude optique radiocristallographique, chimique, Bulletin of the Society of France, Mineralogy and Crystallography, 78, 307–346.

Chou, I. M. (1978) Calibration of oxygen buffers at elevated pressure and temperature using the hydrogen fugacity sensor. American Mineralogist, 63, 650–703.

Chou, I. M. and Williams, R. J. (1977) Hydrogen fugacity sensor measurements of the quartz–fayalite–magnetite and hematite–magnetite buffer reactions (abs.) EOS, 56, 520.

Darken, L. S. and Gurry, R. W. (1964) The system iron–oxygen. II. Equilibrium and thermodynamics of liquid oxide and other phases. Journal of the American Chemical Society, 68, 798–816.

Duffy, C. (1977) Phase Equilibria in the System MgO–MgF_2–H_2O–SiO_2. Ph.D. Thesis, University of British Columbia.

Fender, B. E. F. and Riley, F. D. (1969) Thermodynamic properties of $Fe_{(1-x)}O$ transitions in the single phase region. Journal of Physical Chemistry of Solids, 30, 793–798.

Hansen, M. (1958) Constitution of binary alloys. Second Ed., McGraw-Hill, New York.

Huebner, J. S. (1971) Buffering techniques for hydrostatic systems at elevated pressures. In G. C. Ulmer, Ed., Research Techniques for High Pressure and High Temperature, p. 123–178. Springer-Verlag, New York.

Huebner, J. S. (1975) Oxygen fugacity values of furnace gas mixtures. American Mineralogist, 60, 815.

Huebner, J. S. and Sato, M. (1970) The oxygen fugacity–temperature relationships of manganese oxide and nickle oxide buffers. American Mineralogist, 55, 934–952.

Katsura, T., Kitayama, K., Aoyagi, R., and Sasajima, S. (1976) High temperature experiments related to Fe–Ti oxide minerals in volcanic rocks. In Kazan (Volcanoes) Volume 21, p. 31–56.

Koch, F. B. and Cohen, J. B. (1969) The defect structure of $Fe_{(1-x)}O$. Acta Crystallographia, B25, 275–287.

Lindsley, D. H. (1962) Investigations in the system FeO–Fe_2O_3–TiO_2. Carnegie Institution of Washington Year Book, 61, 100–106.

Lindsley, D. H. (1963) Fe–Ti oxides in rocks as thermometers and oxygen barometers. Carnegie Institution of Washington Year Book, 62, 60–65.

Lindsley, D. H. (1976a) Experimental studies of oxide minerals. In D. Rumble III, Ed., Mineralogical Society of America Short Course Notes, Volume 3, Oxide Minerals, p. L 61–L88.

Lindsley, D. H. (1976b) The crystal chemistry and structure of oxide minerals as exemplified by the Fe–Ti oxides. In D. Rumble III, Ed., Mineralogical Society of America Short Course Notes, Volume 3, Oxide Minerals, p. L1–L60.

Lindsley, D. H. (1981) Some experiments pertaining to the magnetite-ulvospinel miscibility gap. American Mineralogist, 66, 759–762.

Myers, J. and Gunter, W. D. (1979) Measurement of the oxygen fugacity of the cobalt–cobalt oxide buffer assemblage. American Mineralogist, 64, 224.

Neel, L. (1955) Some theoretical aspects of rock magnetism, Advances in Physics, 4, 191–243.

O'Donovan, J. B. and O'Reilly, W. (1979) The temperature dependent cation distribution in titanomagnetites–an experimental test. Physics and Chemistry of Minerals, 5, 235–243.

O'Reilly, W. and Banerjee, S. K. (1965) Cation distribution in titanomagnetites $(1\text{-}x)Fe_3O_4$-xFe_2TiO_4. Physics Letters, 17, 237–238.

Powell, R. and Powell, M. (1977) Geothermometry and oxygen barometry using coexisting iron-titanium oxides: a reappraisal. Mineralogical Magazine, 41, 257–263.

Price, G. D. (1981) Subsolidus phase relations in the titanomagnetite solid solution series. American Mineralogist, 66, 751–758.

Rizzo, H. F., Gordon, R. S., and Cotler, I. B. (1969) The determination of phase boundaries and thermodynamic functions in the iron–oxygen system by EMF measurements. Journal of the Electrochemical Society, 116, 266–274.

Robie, R. A., Hemingway, B. S., and Fisher, J. R. (1978) Thermodynamic Properties of Minerals and Related Substances. U. S. Geological Survey Bulletin 1452, U. S. Government Printing Office, Washington, D. C.

Rumble III, D. (1970) Thermodynamic analysis of phase equilibria in the system Fe_2TiO_4–Fe_3O_4–TiO_2. Carnegie Institution of Washington Year Book, 69, 198–207.

Rumble III, D. (1977) Configurational entropy of magnetite–ulvöspinel$_{ss}$ and hematite–ilmenite$_{ss}$. Carnegie Institution of Washington Year Book, 76, 581–584.

Spencer, K. J. and Lindsley, D. H. (1978) New experimental results on the magnetite–ulvöspinel, hematite–ilmenite solution model using the Co–CoO buffer. Geological Society of America Abstracts with Program, 10, 496.

Stephenson, A. (1969) The temperature dependent cation distribution in titanomagnetites. Geophysical Journal of the Royal Astronomical Society, 18, 199–210.

Taylor, R. W. (1964) Phase equilibrium in the system FeO–Fe_2O_3–TiO_2 at 1300°C. American Mineralogist, 49, 1016.

Thompson, Jr., J. B. (1967) Thermodynamic properties of simple solutions. In P. H. Abelson, Ed., Researches in Geochemistry, p. 340–361. John Wiley and Sons, New York.

Vallet, M. P. (1975) Sur les proprietes thermodynamiques de la wustite solide au-dessous de 911°C. Royal Academy of Science of Paris, Series C, 280.

Vincent, E. A., Wright, J. B., Chevallier, R., and Mathieu, S. (1957) Heating experiments on some natural titaniferous magnetites. Mineralogical Magazine, 31, 624.

Waldbaum, D. R. (1973) The configurational entropies of Ca_2Mg-

Si_2O_7–$Ca_2SiAl_2O_7$ melilites and related minerals. Contributions to Mineralogy and Petrology, 39, 33–54.

Webster, A. H. and Bright, N. F. H. (1961) The system iron–titanium–oxygen at 1200°C and oxygen partial pressures between 1 atmosphere and 2×10^{-14} atmospheres. American Ceramical Society Journal, 44, 110–116.

Wechsler, B. A. (1978) Crystal structure of ilmenite at high temperature. Geological Society of America Abstracts with Program, 10, 513.

Wechsler, B. A. (1981) Crystallographic Studies of Titanomagnetite and Ilmenite. Ph.D. Thesis, State University of New York at Stony Brook, New York.

Manuscript received, October 24, 1980;
accepted for publication, July 15, 1981.

Appendix 1
New experimental results of Mt–Ilm phase equilibria using the Co–CoO oxygen buffer

Experiments using the Co–CoO buffer (which lies between FMQ and WM in its imposed oxygen fugacity) were carried out to test existing oxide models and to produce data in a section of T–f_{O_2}–X space that was previously not accessible to well-calibrated oxygen buffers.

Single-phase starting compositions of Mt_{ss} and Ilm_{ss} were chosen to bracket the tie lines predicted for Co–CoO buffer by interpolation from existing data. Phases of these compositions were prepared by dry-firing mechanical mixes prepared from Fe_2O_3 (J.M. #S5040B), Fe^0 "sponge" (J.M. #S4108-"A"), and TiO_2 (J.M. #B2326) in evacuated silica glass tubes lined with silver foil at ~930°C for 1–2 weeks. This material was then X-rayed and optically examined to determine whether all starting material had reacted to form single, well-crystallized phases, and was reground and re-heated when necessary. Each experimental charge was prepared by grinding together mechanical mixes of these Mt_{ss} and Ilm_{ss} phases. Two such mixtures, of similar bulk composition but significantly different phase composition bracket the expected equilibrium phase compositions.

Table A-1

Run	T(°C)	fO_2*	Starting Composition Usp	Starting Composition Ilm	Run Duration (Hr)	Inner Capsule Material	Run Products (microprobe) Usp	Run Products (microprobe) Ilm
1	600	-20.55	10	100	6761	AgPd	14.5	96.0
2	600	-20.55	25	90		AgPd	--	94.0
3	650	-19.04	10	100	1801	AgPd	38.5	95.3
4	650	-19.04	55	90		AgPd	41.0	94.0
5	700	-17.68	40	100	1159	AgPd	43.0	95.7
6	700	-17.68	55	90		AgPd	44.0	94.0
7A	750	-16.46	50	100	496	AgPd	50.3	95.5
8A	750	-16.46	60	90		AgPd	50.7	92.5
9	800	-15.35	55	100	100	AgPd	55.5	95.5
10	800	-15.35	70	90		AgPd	56.1	92.0
11A	850	-14.33	55	100	69	AgPd	60.7	94.5
12A	850	-14.33	70	90		AgPd	62.0	93.0
13B	900	-13.41	60	100	12.5	Ag	65.3	94.8
14B	900	-13.41	80	90		Ag	66.5	92.5
15	980	-12.08	70	100	3	AgPd	70.2	94.8
16	980	-12.08	90	90		AgPd	72.2	93.0
17	950	-12.56	60	100	2	AgPd	69.4	94.5
18	950	-12.56	80	90		AgPd	69.7	92.8
17A	938	-12.76	60	100	2.25	Ag	68.0	94.5
18A	938	-12.76	80	90		Ag	67.9	92.1
19	900	-13.41	60	100	17.5	AgPd	64.5	94.4
20	900	-13.41	80	90		AgPd	65.5	93.2
21	980	-12.08	60	100	1	AgPd	70.9	94.2
22	980	-12.08	80	90		AgPd	70.4	93.0

* Chou (1978) values.

Experiments were performed using cold-seal pressure vessels loaded into horizontal resistance furnaces (see Huebner, 1971). Pressure for all runs was 1 kbar ±50 bars water pressure. The external pressure medium was H_2O for all runs except those at 950° and 980°, which were done in a TZM bomb using argon gas a pressure-transmitting medium. Water was loaded into all capsules as an internal pressure medium and as an agent for H_2 diffusion. Temperature was monitored using chromel-alumel thermocouples connected to a strip-chart recorder, and checked daily against a potentiometer.

Experiments were done in pairs using the two bracketing (Mt_{ss} + Ilm_{ss}) mixes (Table A-1). Two $Ag_{80}Pd_{20}$ or Ag_{100} capsules were loaded with a mechanical mix of Mt_{ss} + Ilm_{ss} plus approximately 5 to 10 μl of H_2O, welded shut, and then loaded with H_2O and buffer into a single outer Au capsule, which was then also welded shut. Outer capsule length was ~38 mm, less than the length of the hot spot in the pressure vessel.

Quenching was accomplished by removing the vessel from the furnace and blowing compressed air over it for 3–5 min, followed by further slow cooling in air. Capsules were checked for the presence of H_2O and all solid components of the buffer assemblage; the experiments were repeated if the buffer had expired or water was not detected. Runs deemed not to have reached equilibrium were re-run using fresh buffer.

One problem not foreseen was the alloying of Co metal in the buffer with Pd from the $Ag_{80}Pd_{20}$ capsules in high-temperature runs. Hansen (1958) shows extensive solid solution between Co and Pd. As this could alter the effective f_{O_2} imposed on the experimental charge (by diluting Co metal near the

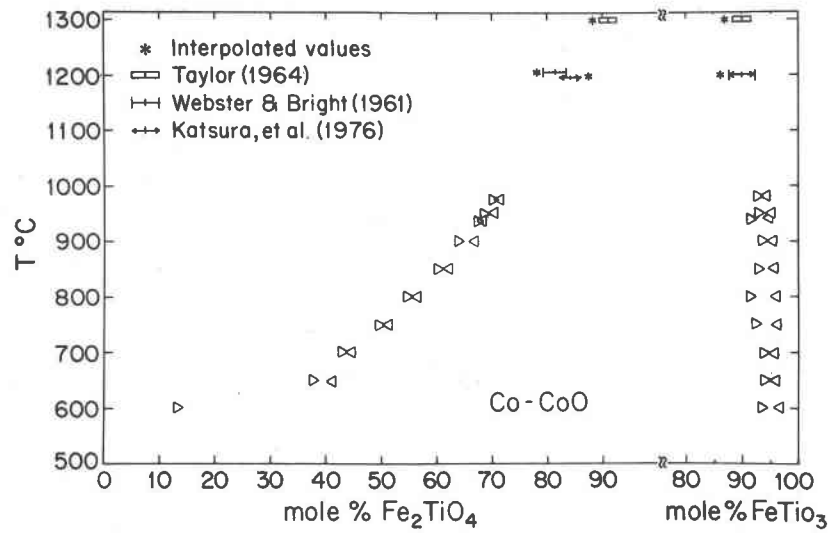

Fig. A-1. Results of experiments done using the Co–CoO oxygen buffer. Left side of diagram is composition of Usp_{ss}(Ilm), right side is Ilm_{ss}(Usp). Our interpolated estimates of the Webster and Bright (1200°C), and Taylor (1300°C) values are also included.

charge or altering the permeability to H_2), several runs were re-done in Ag_{100} capsules, because Ag and Co have very low mutual solubility (Hansen, 1958). Results of these experiments agree with the earlier $Ag_{80}Pd_{20}$ runs.

Analytical procedure

Run products were analyzed by both electron microprobe and a Picker powder X-ray diffractometer using Cu$K\alpha$ radiation and an internal CaF_2 standard (a = 5.4626Å). The Ilm_{ss} (1.0.10), (214), (116), and (204) and Mt_{ss} (622), (533), (620), (440), (333), and (422) peaks were used to determine compositions based on calibration curves (Lindsley, unpublished) for synthetic Mt_{ss} and Ilm_{ss}.

All microprobe analyses were done on an ARL-EMX-SM microprobe at 15 kV, 0.015μA, 400,000 count beam integration, using synthetic Usp 50, Ilm 90, and Ilm 95 as working standards. On-line data reduction was done on a PDP—11 computer using the Bence and Albee (1968) and Albee and Ray (1970) matrix correction procedure. Fe^{3+} was calculated by assuming R_3O_4 and R_2O_3 stoichiometries.

Compositions obtained by electron probe microanalysis were accepted in most cases (Fig. A-1). Some experiments resulted in extremely finely intergrown phases as a result of internal equilibration (oxidation-reduction) of starting phases, and for these, X-ray results gave much more reliable results. Table A-1 shows all successful runs, starting materials, T, f_{O_2}, and run products.